CHEMISTRY OF MATERIALS

pubs.acs.org/cm Article

Surface-Induced Deprotonation of Thiol Ligands Impacts the Optical Response of CdS Quantum Dots

Levi Lystrom, Alyssa Roberts, Naveen Dandu, and Svetlana Kilina*

Cite This: *Chem. Mater.* 2021, 33, 892−901 Read Online

ACCESS | Metrics & More | Article Recommendations | Supporting Information

ABSTRACT: Cadmium chalcogenide quantum dots (QDs) passivated by thiol-based ligands exhibit several advantages in their applications in lighting, sensing, and imaging technologies. However, their emission is sensitive to thiol concentrations, pH conditions, and temperatures. Using calculations based on the density functional theory, we identify conditions for thiol/thiolate equilibrium at the CdS QD surface that either eliminate or introduce optically inactive hole trap states favoring or disfavoring the emission. Our calculations indicate much weaker interactions between the QD and protonated species (thiols), compared to their deprotonated counterparts (thiolates). Additionally, the surface of CdS QD facilitates the partial deprotonation of thiols, leading to the formation of an additional stable networking conformation where the proton is shared between the ligand and the QD surface. Thiolates strongly reduce the optical intensity of low-energy transitions in CdS QDs, contributing thiolate-localized hole trap states at the QD band gap. However, networking between the thiols and the surface, as well as the presence of native ligands such as primary amines, stabilize such trap states brightening the lowest optical transitions. This explains the increased emission of thiol-passivated QDs at lower concentrations in neutral or acidic solutions. Surface-mediated bias toward deprotonated species and their contribution to optically inactive states also rationalizes irreversible emission quenching and bleaching in the CdSe/CdS QDs exposed to high temperatures or intensive laser pulse.

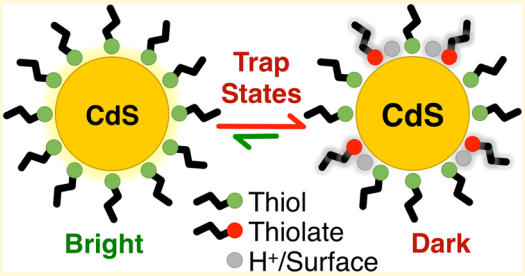

1. INTRODUCTION

Significant research efforts have been focused on the photophysics of colloidal semiconductor quantum dots (QDs). This is motivated by a wide range of QD-based applications such as light-emitting diodes, photosensors, and imaging technologies.[1−4] The ease of synthesis of monodisperse QDs,[5−8] photostability,[9−11] narrow line-width,[12] high quantum yield of emission,[13] and tunability of optical properties via the QDs' size[14−17] make QDs particularly appealing for optoelectronic applications. However, the main challenge of QD-based materials is the sensitivity of QDs' optical response to their surface chemistry and environment.[18,19] For instance, passivating ligands that are in a dynamical equilibrium with the QDs' surface together with charging/discharging of the QD cause intermissions in the emission, known as blinking.[10,11]

The problem of the surface sensitivity has been partially resolved by covering the QD surface with many layers of large band gap semiconductors, so called "giant" core/shell QDs.[2,9] In particular, the CdSe/CdS core/shell QDs can be synthesized via successive ionic layer adsorption and reaction (SILAR). In SILAR, the process of adding monolayers of cations and anions is assisted by injecting cadmium oleates and trioctylphosphine sulfides.[2,21−23] An alternative method, high-temperature continuous injection (HTCI),[12] is based on the continuous injection of cadmium oleates and octanethiols.[12,20] Recent studies comparing the core/shell QDs synthesized by SILAR to HTCI demonstrate different thermally assisted photo-bleaching, ultimately resulting in a more rapid photo-degradation of HTCI-made QDs under high temperatures and laser flux conditions.[20] This difference is rationalized by permanent morphological changes originating from surface ligands. Thiol ligands in HTCI-made QDs promote the irreversible surface/ligand-associated hot-carrier trapping in comparison to the reversible QD charging of SILAR-designed QDs that only have oleate passivation.[20]

However, the origin of such surface/ligand trap states is not completely understood. In fact, in CdSe/ZnS QDs, the surface treatment by thiol derivatives, such as 3-mercaptopropionic acid[24] and β-mercaptoethanol,[4] results in emission enhancement at low concentrations and in acidic conditions. In contrast, a dramatic decline in emission is observed in basic solutions that result in deprotonated species that points to thiolate-originated hole trap states.[4] Nonetheless, neutral and highly acidic conditions have been found insufficient to conclude whether protonated species are responsible for the

Received: September 8, 2020
Revised: December 30, 2020
Published: January 19, 2021

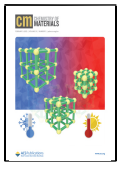

https://dx.doi.org/10.1021/acs.chemmater.0c03610
Chem. Mater. 2021, 33, 892−901

observed emission enhancement, pointing on an optimal thiolate presence together with thiols that provide highly emissive QDs.[4] Despite this unclear effect of thiol ligands resulting in favorable or unfavorable conditions for the QD emission, depending on ligand concentration, pH conditions, temperature, and laser flux intensity, the thiol-based passivation of QDs promises benefits in various applications; this includes device fabrication due to the tight packing of QDs into arrays[25] and bioimaging, since thiol-based ligands can be easily exchanged to polymeric imidazole ligands making the QD water soluble.[12] Therefore, understanding the effect of the thiol/thiolate equilibrium in regard to the formation of surface-associated trap states is critical for the fabrication of highly emissive, nonblinking, and photostable QDs.

Targeting this goal, we computationally study the influence of the protonated and deprotonated thiol-based species on the ground- and excited-state properties of magic size $(CdS)_{33}$ QDs. Understanding the conditions governing the thiol/thiolate equilibrium for this model system helps to determine an optimal interplay between the thiolates and thiols that eliminates hole trap states and favors emission in QDs. The initial structures of magic size[26,27] $(CdS)_{33}$ QD are constructed by cutting quasi-spherical QDs from the bulk CdS wurtzite crystal with a diameter of ∼1.5 nm, as was reported in previous works.[19,28−34] This model is used to represent stoichiometric surfaces with an equal number of surface cadmiums and sulfurs that likely prevail over nonstoichiometric Cd-enriched surfaces in larger size QDs.[8] Since in experiments the thiol passivation takes place via ligand exchange in the presence of prime-amine ligands,[4,24] a relatively lower concentrations of thiol/thiolate ligands is not expected to result on highly nonstoichiometric structures due to the L-type nature of amine ligands.[5]

The resulted initial geometry of $(CdS)_{33}$ QD has a C_3 symmetry and 21 surface cadmium and sulfur ions, Figure 1a. Surface Cd ions are marked according to their layer position in the crystal, with layers A and C having the most reactive two-coordinated ions and layers B and D having three-coordinated atoms that are expected to be less reactive.[35,36] To investigate the effect of thiol ligands, we consider three surface-passivating schemes: (i) a bare $(CdS)_{33}$ QD with a single neutral methanethiol (Thiol) or methanethiolate (Thiolate) with a negative charge of −1 e, attached to one of the surface Cd ions at the layers A−D, Figure 1b. We also consider the case of one methanethiolate attached to the surface Cd and a proton to the neighboring S at the QD surface (Thiolate/H), as illustrated in Figure 1e,f. (ii) Fully passivated $(CdS)_{33}$ QD with 20 methylamines (MA) and one thiol, or thiolate, or thiolate/H attached to the surface Cd ions. (iii) Fully passivated $(CdS)_{33}$ QD with 21 thiols (21-Thiol) or thiolate/H (21-Thiolate/H), Figure 1d.

2. RESULTS AND DISCUSSION

The overall trends in the QD−ligand binding energies are similar for both strongly polar and weakly polar solvents and only slightly deviate between the surface passivation schemes with and without MA, Figure 2. Independent on the surface layer and the presence of MA ligands, thiolate binds to the QD significantly stronger than thiol, while the appearance of a proton on the adjacent surface sulfur provides additional stabilization of the QD−thiolate binding energy. This trend is rationalized by the additional charge−charge and charge−dipole attractions contributing to the dipole−dipole interactions in the structures with thiolate ligands. The more polar

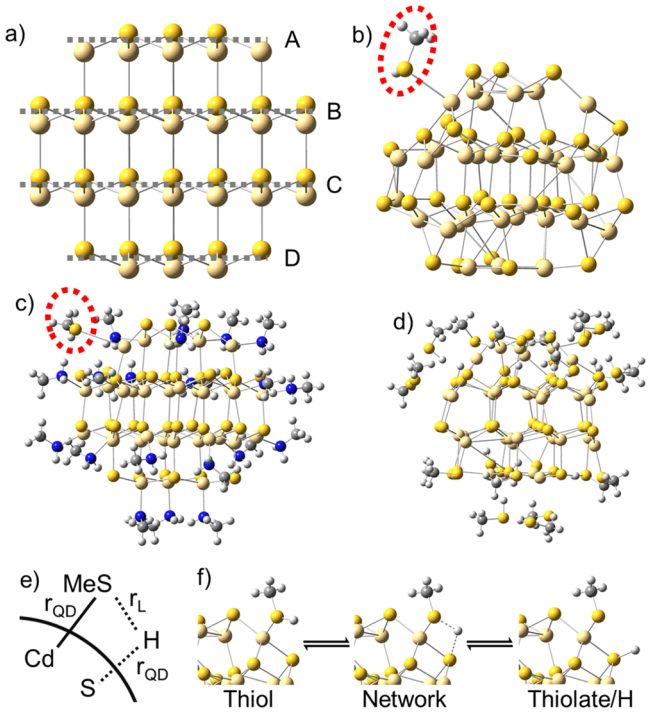

Figure 1. Examples of simulated QD models. (a) Initial structure of $(CdS)_{33}$ QD cut from the bulk wurtzite crystal, with dashed gray lines denoting the surface layers A−D. (b) Optimized structure of the QD with a single thiol bound to the surface cadmium at the layer A. (c) Optimized structure of the QD fully passivated with 20 MAs and one thiol at the layer A. (d) Optimized structure of the QD fully passivated by 21 thiols. (e) Schematic diagram illustrating three bonds that define the interaction between the QD and thiol/thiolate ligands and formation of the thiol/thiolate network with the surface. (f) Interconversion between thiol and thiolate where the QD extracts H^+ due to its attraction to the surface sulfur.

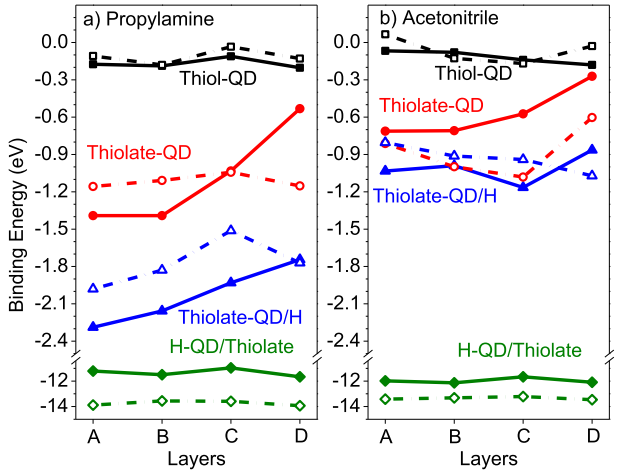

Figure 2. Binding energy of the thiol and thiolate ligands to the $(CdS)_{33}$ QD in PAM (a) and ACN (b) solvents as a function of their position at the surface layers A−D. Solid lines represent the QD passivated by 20 MAs and one thiol (black), thiolate (red), or thiolate-H with QD−thiolate (blue) and QD−H (green) binding energies. Dashed lines represent the QD passivated by a single thiol (black), thiolate (red), or thiolate/H (blue or green).

solvent such as acetonitrile (ACN) reduces the strength of the QD−thiolate interaction (by about 2 times) when compared to the less polar propyl-amine (PAM) solvent. This is expected

https://dx.doi.org/10.1021/acs.chemmater.0c03610
Chem. Mater. 2021, 33, 892−901

because these types of interactions are inversely proportional to the dielectric constant of the media.[37] In contrast, the polarity of the solvent only slightly affects the QD−thiol interaction in the neutral structures.

The QD−thiol interaction is also much less dependent on which surface (layer) the molecule is attached to the QD, compared to the QD−thiolate binding energy, Figure 2. The interaction between the QD and thiolate is the strongest for the A-layer attachment and the weakest is the D-layer. This trend is more pronounced for the structures fully passivated with MAs and well rationalized by the more reactive character of two-coordinated cadmium ions at the A-layer when compared to three-coordinated cadmiums at the D-layer, as was found for the $(CdSe)_{33}$ QDs bound to different types of surface ligands.[35,38] The deviations from this trend for structures passivated with only one thiolate (red and blue dashed lines in Figure 2) can be explained by stronger surface reconstructions of the bare QD making all surface cadmium ions three-coordinated, thus reducing the difference between layers.[35] Similar to the QD−thiol binding energy, the interaction between a proton and the sulfur ions at the QD surface (green lines in Figure 2) has insignificant dependence on the layer attachment and the solvent, despite its significant strength. The strong H−S bond results in electron density redistribution, making the charge on H-side only slightly positive, like the proton in the thiol molecule (Figure S1 and Table S1 in Supporting Information), which explains the similarity in their trends of the binding energies.

The decrease in the interaction strength between the QD and thiol compared to the QD and thiolate agrees with the trend of the Cd−S bond length between the surface cadmium and sulfur of the ligand, Figures 3a and S2a. For the thiol, the Cd−S bond length is significantly longer (3.4−3.8 Å) than for the thiolate (2.6−2.7 Å). This difference agrees with the less polar character of the Cd−S bond of the thiol, compared to those of the thiolate, Table S1. The difference in the Cd−S bond length and its polarity results in a weaker interaction between the QD and the thiol than the QD and the thiolate. As such, the deprotonation of thiol ligands, if it occurs, results in a very stable passivation of the QD surface by thiolates at their lower concentration. The stability is further facilitated by the proton attachment to the nearest sulfur at the QD surface. Both processes are more thermodynamically favorable in less polar solvents, Figure 2.

Interestingly, the distance between H in the thiol and S in the QD (r_{QD}, Figure 1e) noticeably decreases for the thiol attachment at the C-layer in the PAM solvent, while the H−S bond length between H and S of the thiol (r_L, Figure 1e) only slightly increases, as can be seen in Figure 3b. Similarly, the distance between H adsorbed at the QD surface and S in the thiolate (r_L) also strongly reduces when the thiolate is attached at the C-layer in the Thiolate/H conformation, Figure 3c. These trends are consistent for the QDs with MA passivation (Figure 3b,c), as well as the bare QDs with only one thiol or thiolate/H at the surface, Figure S2b,c. A strong reduction of r_{QD} for the Thiol structure and r_L for the Thiolate/H structure at the C-layer attachment is a signature of the network formation when the proton is interacting with both sulfurs from the ligand and the QD, as illustrated in Figure 1e,f. The edge between layers C and D favors the interaction between the capping thiol (thiolate) in layer C and the surface sulfur (with attached H) in layer D, resulting in the networking configuration. Note that this network configuration does not represent the complete conversion of the thiol to the thiolate/H or vice versa, as evidenced by a larger Cd−S bond length (~3 Å) of such networking thiol, compared to the typical Cd−S bond length (2.5−2.7 Å) between the thiolate and the QD, Figures 3a and S2a. As such, our simulations reveal an additional stable conformation of the thiol/thiolate networking between the ligand and the surface, which can take place together with completely protonated thiols or deprotonated thiolates.

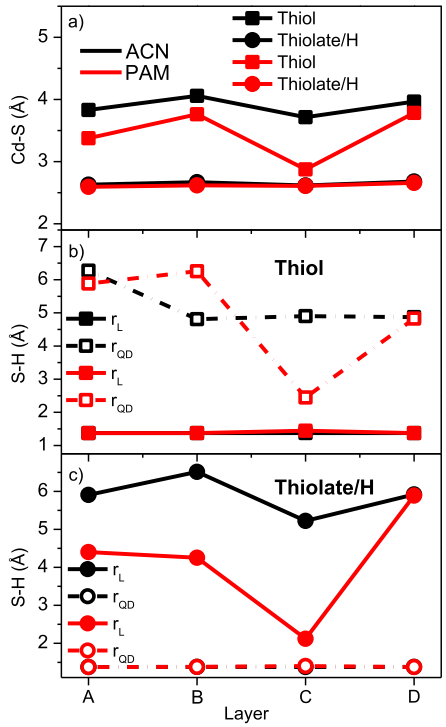

Figure 3. Cd−S and S−H bond lengths of fully passivated $(CdS)_{33}$ QDs with 20 MAs and one thiol or thiolate/H as a function of their position at the surface layers A−D in PAM (red lines) and ACN (black lines). (a) Cd−S bond length between surface Cd and S of the thiol (circles) or thiolate (squares). (b) Distance between H and S in the thiol (solid line, r_L) and S in the QD surface (dashed line, r_{QD}) of the Thiol structure. (c) Distance between H and S in the thiolate (solid line, r_L) and S in the QD surface (dashed line, r_{QD}) of the Thiolate/H structure. A noticeable reduction in r_{QD} for the Thiol structure and r_L for Thiolate/H structure at the C-attachment points to the network formation when the proton is interacting with sulfurs from both the ligand and the QD.

The protonated and deprotonated thiol-based ligands at the QD surface are expected to alter the electronic structure and optical response of CdS QDs in different ways. For instance, it has been detected experimentally that the emission efficiency of pristine CdSe, core/shell CdSe/ZnS, and CdSe/CdS QDs strongly depends on the pH of the solution and the concentration of the thiol-based ligands.[4,20,24] The calculated density of states (DOS) projected to the electronic states originating from QDs, MAs, and thiol/thiolates are shown in Figure 4 for the attachment at the layer A and Figures S3−S5 for other layers. The passivation of the QD by pristine amines insignificantly affects the QD states. States associated with MAs appear deep inside the valance band (VB) and conduction band (CB), independent of the solvent and the form, protonated or deprotonated, of the thiol-based ligand.

https://dx.doi.org/10.1021/acs.chemmater.0c03610
Chem. Mater. 2021, 33, 892−901

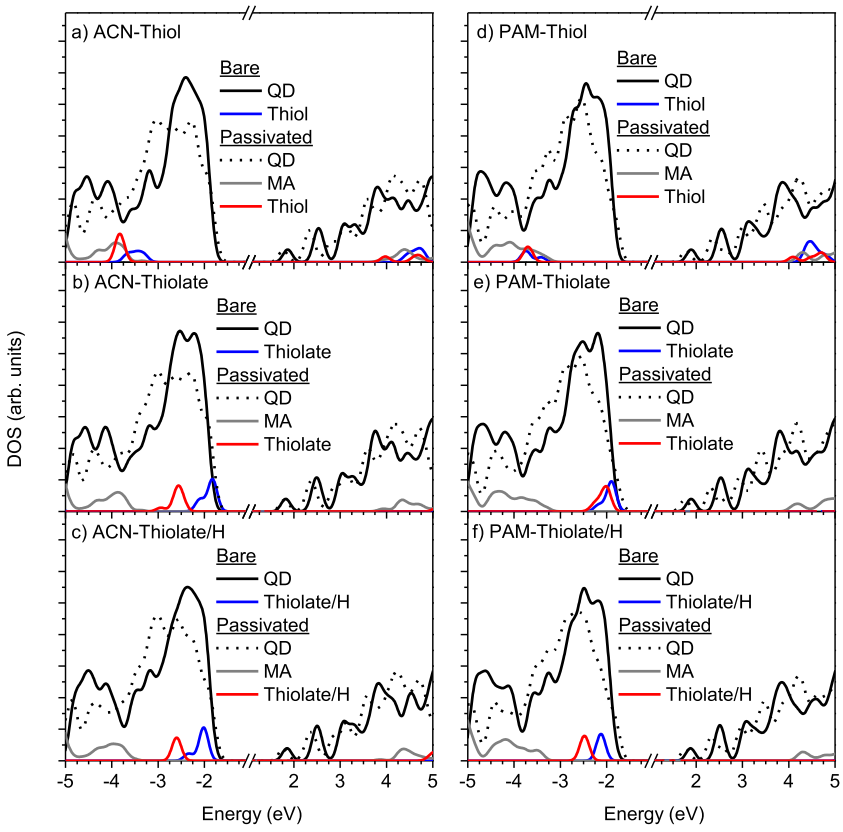

Figure 4. DOS projected to the orbitals originated from the $(CdS)_{33}$ QD, thiol, thiolate, thiolate/H, and MA in the bare QD with only one thiol-based ligand and fully passivated QD by 20 MAs and one thiol-based ligand attached at the layer A. The panels (a−c) represent DOS in ACN and (d−f) in PAM solvents. The DOS contribution of the thiol, thiolate, and thiolate/H are multiplied by 3 for better visualization. (a,d) Structures with thiol, (b,e) structures with thiolate, and (c,f) structures with thiolate/H.

These results are consistent with reports on CdSe QDs passivated by primary amines.[36]

In both solvents, electronic states originated from the thiol also contribute only deep inside the VB and CB close to the amine-associated states (Figure 4a,d) and are nearly independent on the thiol position at the surface (Figures S3−S5). In contrast, the thiolate-associated states for the Thiolate and Thiolate/H structures appear much closer to the VB edge or at the VB edge, Figure 4b,e. This trend is similar for all cases except when thiolate binds to the bare QD on the layer C, Figure S4b,e, where the thiolate states shift toward the amine-associated states. This migration can be explained by the bridging of thiolate between two surface Cd ions, which stabilizes the ligand states.

A similar trend has been observed in CdSe QDs functionalized by metal−organic complexes where the states originating from the neutral ligands of the complex are strongly stabilized and appear deep inside the QD's VB, while anionic ligands destabilize these states shifting them to the edge of the QD's VB.[32,39−41] This destabilizing behavior is rationalized by the increased dipole−dipole interactions between the QD surface and the ionic ligands, compared to neutral ligands.[40] For our systems, this trend is the most pronounced for structures without MA passivation, where the thiolate-associated state is located exactly at the VB edge (blue lines in Figure 4b,e). As such, the surface ligands stabilize the thiolate-associated states. The proton attached to the QD surface also stabilizes the thiolate-associated states of the Thiolate/H structures via reducing the dipole moment of the QD surface, Figures 4c,f and S3−S5.

For all considered structures, independent of the solvent, the excited electron state contributing to the lowest energy optical transition is highly delocalized over the entire QD, Figures 5 and S6. This is consistent with the nature of the CB edge of their DOS, Figure 4. For the bare QDs with one thiolate in PAM solvent, the thiolate-associated states at the VB edge contribute to the hole of the first excited state, which is optically inactive due to its ligand-to-QD charge-transfer character, Figure 5a,c. However, stabilization of the thiol-/thiolate-associated states due to passivating amine ligands and/or the surface proton results in the QD-to-QD lowest transition that is optically active in Thiol and Thiolate/H structures for the bare and amine-passivated QDs, Figure 5b,d. It is important to note, however, that the polar ACN solvent leads to a stronger delocalization of the hole state between the thiolate and the QD (with a larger portion at the QD), resulting in an optically active lowest energy transition in the thiolate structure, despite the thiolate contribution to the hole state, Figure S6a,c. On the other hand, the polar solvent changes the symmetry of the hole state contributing to the lowest QD-to-QD transition, which significantly reduces its optical intensity in all structures passivated by primary amines. The change in the symmetry of the hole arises from the orientation of the ligands on layer C so that they partially stabilize S ions in layer D, resulting in the localization of the hole on layer D. In fact, when the hole state is delocalized over the B-layer, such as in PAM, the transition is optically

https://dx.doi.org/10.1021/acs.chemmater.0c03610
Chem. Mater. 2021, 33, 892−901

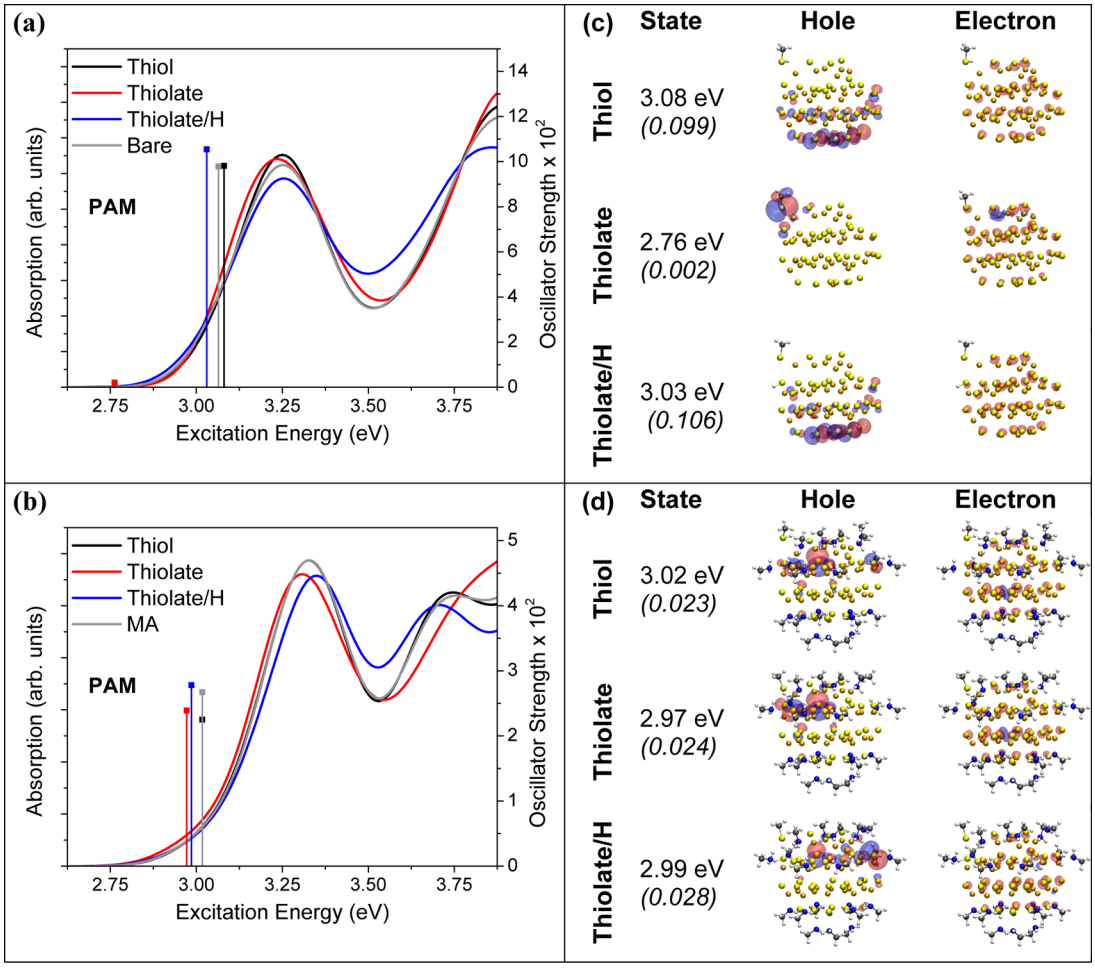

Figure 5. Absorption spectra and NTOs representing the electron−hole pair contributing to the lowest optical transition of the bare QD with only one thiol-based ligand (a,c) and fully passivated QD by 20 MAs and one thiol-based ligand (b,d) attached at the layer A and calculated in PAM. As a reference, the spectra of the bare $(CdS)_{33}$ QD without any ligands (a) and fully passivated by 21 amines (b) are shown by gray lines. The vertical lines introduce the lowest energy transition for each structure, with its oscillator strength shown at the right *Y*-axis (a,b) and in prentices (c,d).

intensive. In contrast, a distribution of the hole mainly over the D-layer, such as in ACN, results in optically weak transitions (compare Figures 5d to S6d and Table S2). The same change in the character of the hole state and the related optical intensity of the lowest transition between PAM and ACN solvents is observed in QDs passivated only by MAs, explaining noticeably the lower intensity of the first excited state in ACN compared to that in PAM solvents, Table S3.

The attachment of thiol or thiolate to different layers of the QD results in a similar behavior of the lowest energy transitions as discussed for the A-layer, Figures S7, S8, and Table S2. The exception is observed for the C- and D-layers of bare structures, where the hole state is localized on the surface, rather than the inner part of the QD, resulting in an additional red-shifted optically weak band in their absorption spectra, Figures S7f,h, S8f,h, and Table S2. We associate the appearance of these surface states with the network formation when the proton is interacting with sulfurs from both the thiol ligand and the QD. This networking is observed only for layers C and D with a more pronounced character for the bare Thiol and Thiolate/H structures.

Overall, our calculation points to a tendency of passivating thiolates reducing or completely eliminating the optical intensity of the lowest energy transition in CdS QDs, due to the contribution of the trap hole states localized either on the thiolate or on the surface. This effect of "darkening" of the first excited state is weakened when a proton is attached at the QD surface or forming the network between the thiol molecule and the QD surface. The presence of a large amount of neutral passivating ligands such as primary amines (small concentrations of thiolates) also eliminates this effect, due to stabilization of the thiolate-associated states by amines. In contrast to anionic thiolates, neutral thiols at lower concentrations provide a high optical intensity of the first exciton, responsible for the emission. These computational findings agree with experimental results, which report enhanced emission in QDs treated by thiols at low concentrations and acidic environments that favor the protonated species, while emission is strongly reduced at high concentrations and in basic solutions where thiolates dominate over thiols.[4]

To better justify these conclusions, we have simulated a limiting case of a high thiol/thiolate concentration, when the $(CdS)_{33}$ QD is fully passivated either by 21 thiols (21-Thiol) or by 21 thiolates with 21 protons attached to sulfur ions of the QD surface (21-Thiolates/H). Here, we consider acidity as an access of protons in a solution that is expected to strongly facilitate protonation of thiols (21-Thiol model), while the deprotonation of thiols is favored in basic solutions enhancing thiolate/H network formation (21-Thiolates/H model). While

https://dx.doi.org/10.1021/acs.chemmater.0c03610
Chem. Mater. 2021, 33, 892−901

this is, indeed, an implicit consideration of acidity, direct modeling of thiol/thiolate equilibrium in acidic solutions would strongly benefit from the fundamental understanding of how thiol converts into thiolate/H or vice versa due to the QD surface, which we address in these simulations.

After optimization of 21-Thiol structures, majority of thiols have been partially deprotonated, resulting in 18 network species, predominantly with the surface character, where the distance between the proton and the sulfur of the QD surface is slightly smaller, than between the proton and the sulfur from the neighboring ligand, Table 1. To accurately differentiate between the surface- and ligand-network species, we also compare the charge on the sulfur atom of the thiol-based ligand using natural bond orbital (NBO) analysis. Partially deprotonated thiols with the sulfur's charge being in the range of −0.63 to −0.50 e correspond to the surface network (behave more like thiolate species), while those with the less negative charge from −0.16 to −0.07 e contribute to the ligand network (behave more like thiol species). While the overall trend is similar for PAM and ACN solvents showing a bias toward ligand- and surface-network species for 21-Thiol structures, the surface-network species are slightly dominating in the polar solvent (12 in ACN vs 10 in PAM, Table 1). Comparing these results to single thiol passivation, we can also conclude that the interaction between neighboring thiol ligands facilitates network formation and deprotonation trends, including A- and B-layers that do not show such behavior at a single thiol passivation.

Table 1. Number of Final Species at the Surface of $(CdS)_{33}$ QD after Optimization of Initial Structures Completely Passivated Either by Thiols (21-Thiol) or by Thiolates with Protons Attached to the QD Surface (21-Thiolate/H) in Different Solvents

	PAM solvent		ACN solvent	
final species	21-Thiol	21-Thiolate/H	21-Thiol	21-Thiolate/H
thiols	3	0	3	0
thiolate/H	0	14	0	15
surface network	10	7	12	6
ligand network	8	0	6	0

In contrast, the optimization of 21-Thiolate/H structures results in less pronounced changes in both solvents, where the major species (∼2/3) stays as the thiolate and a minority (1/3) exhibits the surface-network character sharing the proton between the QD and the thiolate. From these data, it is reasonable to assume that thiolate/H species will dominate at temperatures high enough to distort the S−H bond of the thiol because the QD surface catalyzes the thiol deprotonation converting it into the thiolate with the proton attached to or sharing with the surface. This process is not thermodynamically reversible, so that deprotonated species do not pose conversion to protonated ones when the temperature is reduced. In contrast, thiols tend to undergo partial deprotonation even in neutral (or acidic) solutions at the normal temperature, where the surface and ligand networks are nearly balanced and a majority of thiols are not completely deprotonated and sharing the proton either with the QD surface or neighboring ligands.

Examining the electronic states originating from the QD, thiol, thiolate/H, and networking between the surface and ligands, as shown in Figure 6a−d, we see that both the thiolate and the surface-network species introduce their states at the VB edge and inside the band gap of the QD. The higher the negative charge of the sulfur of the ligand (having more thiolate character), the greater the shift of the ligand-localized hole trap state inside the band gap of the QD, Figure S9. This results in the lowest energy transitions with a very weak optical intensity for the 21-Thiolate/H structure in both PAM and ACN solvents, Figure 6e,f. Such a "dark" character of the lowest exciton of 21-Thiolate/H structures is rationalized by localization of the hole on thiolates at the D-layer, while the electron is delocalized on the QD core, resulting in the ligand-to-QD charge-transfer nature of the first transition, Table 2. These results are consistent with those obtained for the QD

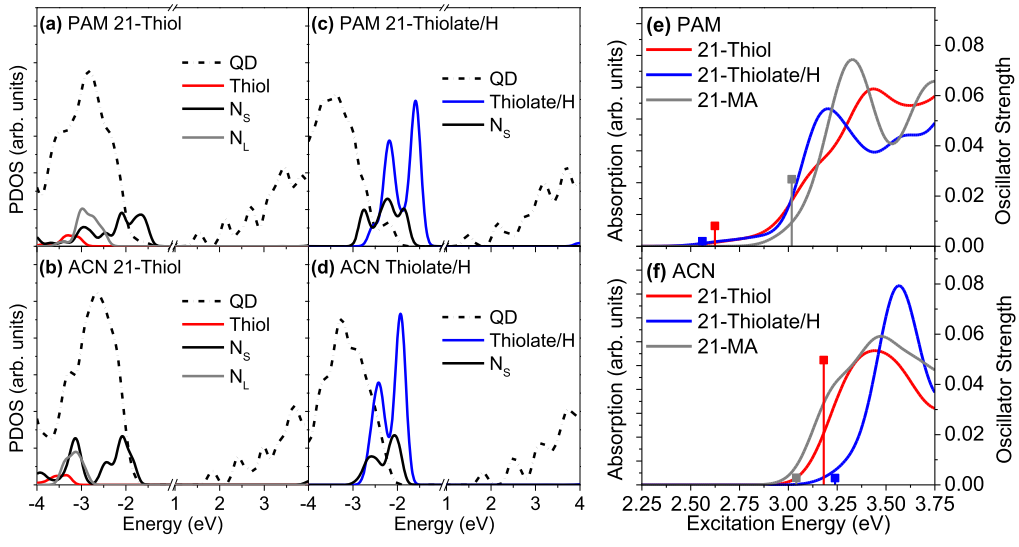

Figure 6. Ground-state and excited-state electronic spectra of $(CdS)_{33}$ QD passivated by 21 thiols and 21 thiolate/H in PAM and ACN solvents. (a−d) DOS projected to different parts of the system: the QD, thiols, thiolates, and the network with a proton shared between the QD and ligands with the smallest H−QD distance called network-surface (N_s) or the smallest H−ligand distance called network-ligand (N_L). (e,f) Absorption spectra of 21-Thiol and 21-Thiolate/H passivated QDs, compared to those of the QD passivated by 21-MA.

https://dx.doi.org/10.1021/acs.chemmater.0c03610
Chem. Mater. 2021, 33, 892−901

Table 2. NTOs Representing the Electron−Hole Pair Contributing to the Lowest Optical Transition and the Next Most Optically Active State of the $(CdS)_{33}$ QD Fully Passivated by 21 Thiols (21-Thiol) and 21 Thiolate/H (21-Thiolate/H) in ACN and PAM Solvents[a]

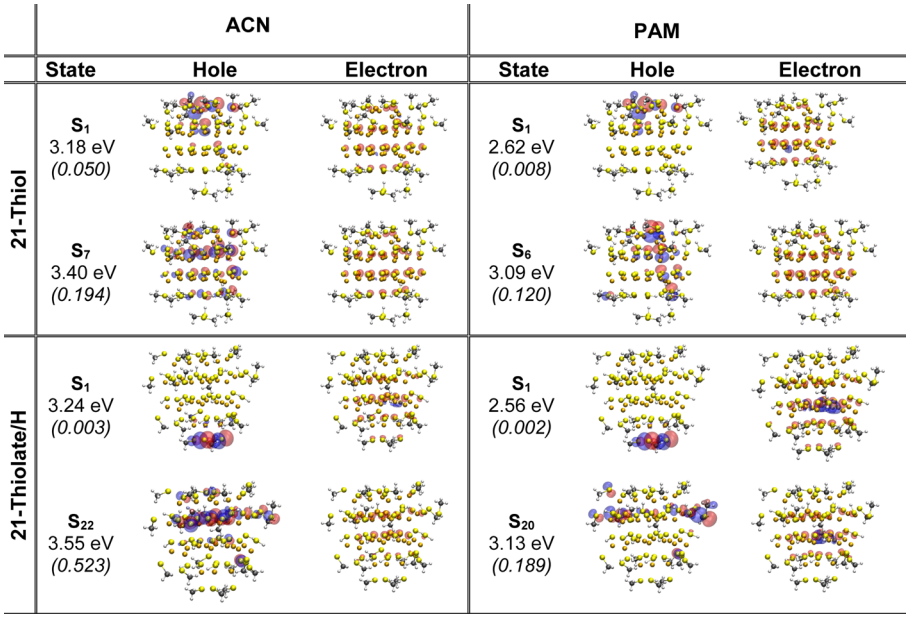

[a]The oscillator strength of the transition is indicated in prentices.

with a single thiolate, Figures 5 and S6. However, the polar solvent stabilizes the occupied states originated from thiolates and/or the surface network, shifting them toward QD's VB. This results in a blue shift of the lowest transitions in ACN for all thiol-/thiolate-containing structures, compared to those in PAM, Figures 6e,f and S10. Additionally, ACN increases the delocalization of the hole states, originated from the surface network, over the ligands and the A- and B-layers of the QD for 21-Thiol, Table 2. As a result, the lowest energy transition of 21-Thiol in ACN is highly intensive (Figures 6f and S10), providing favorable conditions for emission. Similar trends for the DOS and low-energy optical transitions are observed for $(CdSe)_{33}$ QD with 21-Thiol or 21-Thiolate/H passivation (Figure S11), pointing that this behavior is universal for any chalcogenide QDs with thiol ligands.

Note that this condition of full thiol passivation is unlikely to be obtained using the ligand-exchange procedure, as was used in ref 4, because the binding energy of the native ligands, such as primary amines, to the QD is significantly stronger than those of thiols in their protonated form.[35] However, deprotonated species (thiolates and surface network) interact much stronger than native ligands and are likely to dominate the surface passivation at high thiol concentrations, leading to thiolate-associated trap states similar to those observed for the 21-Thiolate/H structures and resulting in emission quenching.[4] In contrast, the CdSe/CdS core/shell QDs designed by the HTCI method, where thiol precursors are used directly during synthesis,[20] are likely to result in a stable thiol/network passivation with the balanced ligand- and surface-network species, like in our 21-Thiol model, which provides optically bright lowest energy transitions beneficial for room-temperature stable emission with high quantum efficiency.[20]

3. CONCLUSIONS

In conclusion, our calculations provide important insights into the thiol/thiolate equilibrium at the surface of CdS QDs that help to explain experimental results demonstrating the dual role of thiols and thiolates in enhancing or decreasing the emission efficiency.[4,20,24] Our calculations reveal that the surface of the QD catalyzes the partial deprotonation of the thiols, leading to the formation of the network where the proton is shared between the ligand and the QD surface. In addition, the interaction between the thiolate and the QD is much stronger than that between the protonated species, while attachment of the proton to or sharing with the QD surface further increases the QD/thiolate interaction. This implies that even in neutral or weakly acidic solutions, deprotonation of the thiol occurs with attachment (or sharing) of the proton to the QD surface, while the conversion back to the protonated species is not thermodynamically favorable. As such, the thiol/thiolate equilibrium is shifted toward thiolates at any conditions while also forming a network where the proton is shared either between the ligand and the QD surface (surface network) or between the neighboring thiolate (ligand network).

In their deprotonated form, thiolates introduce hole trap states inside the band gap of the QD, resulting in optically inactive (or very weak) lowest energy transitions with the ligand-to-QD charge-transfer character. This explains the dramatic reduction in emission efficiency in thiol-passivated QDs in basic solutions and at high concentrations favoring deprotonated species.[4,47,48] In the case of low thiol concentration and polar solvents, however, the native passivating ligands, such as primary amines, stabilize the thiolate-originated hole states shifting them deeper to the QD's VB. Meanwhile, the interplay between the surface- and ligand-network species eliminates electron trap states due to passivating surface sulfurs with protons while also moving the hole trap states away from the QD's band gap. This results in highly intensive lower energy transitions providing favoring conditions for efficient emission at lower thiol concentrations in acidic environments, which agree with experimental

https://dx.doi.org/10.1021/acs.chemmater.0c03610
Chem. Mater. 2021, 33, 892−901

observables.[4,20] However, high temperatures are expected to facilitate the irreversible deprotonation of thiols by the QD surface, so that the surface network is dominating. A high thermodynamic stability of the deprotonated surface-network species and their contributions to optically inactive hole states rationalizes irreversible emission quenching and bleaching in the CdSe/CdS QDs prepared by the HTCI method, when exposed to high temperatures and/or intensive laser pulse.[20] Thus, understanding the conditions governing the thiol/thiolate equilibrium helps to interpret experimental data and determine an optimal interplay between the thiolates and thiols that eliminates hole trap states and favors emission in QDs.

4. METHODS AND COMPUTATIONAL DETAILS

All our calculations are based on the density functional theory (DFT), as implemented in the Gaussian 16 software package.[42] Both the ground- and excited-state calculations are performed using the hybrid functional PBE0[43] with a mixed basis set LANL2DZ[44,45] applied for Cd and S and 6-31g*[46−50] applied for H, C, and N atoms. The conductor-like polarizable continuum model[51,52] is used to implicitly include solvation effects for weakly polar PAM and highly polar ACN solvents. This methodology has been previously applied in modeling ground and excited-state properties of cadmium chalcogenide QDs by our group[16,19,28,30−32,36] and others[29,34] showing qualitative agreement with experimental studies. The ligand−QD binding energy is computed by subtracting the energies of the noninteracting optimized fragments (the pristine QD and the ligand) and the optimized ligand-passivated QD. Negative values of the binding energy indicate chemisorption of ligands at the QD surface, whereas positive values occur for ligands that are weakly physisorbed at the QD surface.

We have investigated the effect of the basis sets and functionals on the QD−ligand binding energy and the electronic structure of the $(CdS)_{33}$ QD with a single Thiol, Thiolate, and Thiolate/H, Figures S12 and S13 in Supporting Information. In agreement with previous literature reports,[53] more extended basis sets used for ligands, such as 6-31^{+}g* and 6-311^{+}g*, reduce the QD−ligand interaction energy by about 0.2 eV, while the long-range corrected functionals, such as ωB97XD and CAM-B3LYP, stabilize the ligand−QD binding energy by 0.15−0.35 eV, compared to the hybrid PBE0 functional. Nonetheless, neither a choice of the functional nor the basis set changes the qualitative trends in the strength of the thiol and thiolate bindings to the QD: the deprotonation of the thiol results in a stronger thiolate/QD interaction than the thiol/QD interaction. This stability is further facilitated by the proton attachment to the nearest sulfur at the QD surface (Thiolate/H). These trends are more pronounced in less polar solvents, since a polar solvent screens the QD−ligand interactions.

We also investigated the effect of the functional on the electronic structure of studied systems, comparing the projected DOS (PDOS) calculated by PBE0, ωB97XD, and CAM-B3LYP functionals, Figure S14 in Supporting Information. As expected, both the states associated with the QD and the states of the thiol and thiolate ligands, as well as their relative alignment are insignificantly affected by the functionals, exhibiting identical trends (see more extended discussion in Supporting Information). As such, we conclude that our choice of the PBE0 functional and LANl2DZ/6-31G* basis set is a reasonable approach providing similar trends in both the ligand−QD binding energies and the electronic structures of the studied systems while taking less computational cost compared to more advanced long-range corrected functionals and extended basis sets. It is also important to note that while the used optimization procedure does not guarantee a global minimum of obtained structures, the consistency in the trends for structures in different solvents and with different thiol concentration (one thiol/thiolate vs full passivation), calculated by different functionals and basis sets, points to a high stability of obtained structures. One can conclude that the probability to get such structures is high enough to compete with other possible conformations of QD samples at room temperature.

The absorption spectra are calculated using linear response time-dependent DFT applying the same functional and the basis set as used in the ground-state calculations. The obtained oscillator strengths and transition energies are broadened by the Gaussian function with a line width of 0.10 eV to reproduce a typical thermal broadening of the absorption spectra.[16] The emissive properties are estimated based on the optical activity of the lowest singlet transition according to the Kasha's rule[54] justified by the small Stokes shifts in QDs.[55] It is well known that the phonon-mediated interband carrier relaxation from the initially excited state to the band edge states, including ligand-/defect-associated states, happens at the picosecond range in small-size QDs, which is much faster than emission (nanosecond range).[18,28] As such, it is reasonable to assume that emission takes place from the lowest state if it is optically active (large oscillator strength), since such radiative electron−hole recombination is much faster than nonradiative recombination via intraband multiphonon processes.[49] However, if the lowest state is optically weak or completely inactive, such as surface/ligand trap states, it takes a much longer time for electron−hole recombination allowing for nonradiative multiphonon relaxation to compete and quench emission. As such, the oscillator strength of the lowest transition (which is proportional to the radiative time) could be used as an estimate of the emission efficiency of the QDs. The nature of the excited states is characterized by natural transition orbitals (NTOs)[56] representing the electron−hole pair contributing to the optical transition and visualized via VMD[57] with an isovalue of 0.02.

■ ASSOCIATED CONTENT

Supporting Information

The Supporting Information is available free of charge at https://pubs.acs.org/doi/10.1021/acs.chemmater.0c03610.

NBO analysis representing the charge on several selected atoms of the $(CdS)_{33}$ passivated by 20 MAs and one thiol, or thiolate, or thiolate/H; Cd−S and S−H bond lengths of the $(CdS)_{33}$ passivated by only one thiol or thiolate/H ligand as a function of the ligand position at the surface layers in different solvents; DOS projected to the orbitals originated from the $(CdS)_{33}$ and passivating ligands in all considered structures with the thiol-based ligand attached at the surface layer B, C, and D; absorption spectra and NTOs of all considered structures with the thiol-based ligand attached at the surface layers A, B, C, and D and calculated in different solvents; PDOS of the $(CdS)_{33}$ passivated by 21 thiol-based ligands; absorption spectra of the $(CdS)_{33}$ passivated by 21 thiol-based ligands in different solvents; ground-state and excited-state electronic spectra of $(CdSe)_{33}$ QD passivated by 21 thiol-based ligands in ACN solvent; and coordinates (*xyz*-format) of the optimized $(CdS)_{33}$ passivated by 20 MAs and one thiolate/H at the A- and C-layers and fully passivated by thiols and thiolate/H in the ACN solvent (PDF)

■ AUTHOR INFORMATION

Corresponding Author

Svetlana Kilina − *Chemistry and Biochemistry, North Dakota State University, Fargo, North Dakota 58108, United States;* orcid.org/0000-0003-1350-2790; Email: skilina@gmail.com, Svetlana.kilina@ndsu.edu

Authors

Levi Lystrom − *Chemistry and Biochemistry, North Dakota State University, Fargo, North Dakota 58108, United States*

Alyssa Roberts − *Chemistry and Biochemistry, North Dakota State University, Fargo, North Dakota 58108, United States*

https://dx.doi.org/10.1021/acs.chemmater.0c03610
Chem. Mater. 2021, 33, 892−901

Naveen Dandu − *Argonne National Laboratory, Lemont, Illinois 60439, United States;* orcid.org/0000-0001-7122-8537

Complete contact information is available at: https://pubs.acs.org/10.1021/acs.chemmater.0c03610

Author Contributions

The manuscript was written through contributions of all authors. All authors have given approval to the final version of the manuscript.

Notes

The authors declare no competing financial interest.

■ ACKNOWLEDGMENTS

The authors thank Dmitri S. Kilin and Jennifer Hollingsworth for fruitful discussions and comments. This material is based upon the work supported by the National Science Foundation under grant no. 2004197. For computational resources and administrative support, the authors acknowledge the Center for Computationally Assisted Science and Technology (CCAST) at North Dakota State University and the National Energy Research Scientific Computing Center (NERSC) allocation award 86678, supported by the Office of Science of the DOE under contract no. DE-AC02-05CH11231. This work was performed in part at the Center for Integrated Nanotechnology (CINT), a U.S. Department of Energy and Office of Basic Energy Sciences user facility at the Los Alamos National Laboratory (LANL).

■ REFERENCES

(1) Dai, X.; Zhang, Z.; Jin, Y.; Niu, Y.; Cao, H.; Liang, X.; Chen, L.; Wang, J.; Peng, X. Solution-processed, high-performance light-emitting diodes based on quantum dots. *Nature* **2014**, *515*, 96−99.

(2) Chen, Y.; Vela, J.; Htoon, H.; Casson, J. L.; Werder, D. J.; Bussian, D. A.; Klimov, V. I.; Hollingsworth, J. A. "Giant" multishell CdSe nanocrystal quantum dots with suppressed blinking. *J. Am. Chem. Soc.* **2008**, *130*, 5026−5027.

(3) Pal, B. N.; Ghosh, Y.; Brovelli, S.; Laocharoensuk, R.; Klimov, V. I.; Hollingsworth, J. A.; Htoon, H. 'Giant' CdSe/CdS core/shell nanocrystal quantum dots as efficient electroluminescent materials: strong influence of shell thickness on light-emitting diode performance. *Nano Lett.* **2012**, *12*, 331−336.

(4) Jeong, S.; Achermann, M.; Nanda, J.; Ivanov, S.; Klimov, V. I.; Hollingsworth, J. A. Effect of the thiol−thiolate equilibrium on the photophysical properties of aqueous CdSe/ZnS nanocrystal quantum dots. *J. Am. Chem. Soc.* **2005**, *127*, 10126−10127.

(5) Morris-Cohen, A. J.; Frederick, M. T.; Lilly, G. D.; McArthur, E. A.; Weiss, E. A. Organic surfactant-controlled composition of the surfaces of CdSe quantum dots. *J. Phys. Chem. Lett.* **2010**, *1*, 1078−1081.

(6) Murray, C. B.; Norris, D. J.; Bawendi, M. G. Synthesis and characterization of nearly monodisperse CdE (E= sulfur, selenium, tellurium) semiconductor nanocrystallites. *J. Am. Chem. Soc.* **1993**, *115*, 8706−8715.

(7) Murray, C. B.; Kagan, C. R.; Bawendi, M. G. Synthesis and characterization of monodisperse nanocrystals and close-packed nanocrystal assemblies. *Annu. Rev. Mater. Sci.* **2000**, *30*, 545−610.

(8) Wei, H. H.-Y.; Evans, C. M.; Swartz, B. D.; Neukirch, A. J.; Young, J.; Prezhdo, O. V.; Krauss, T. D. Colloidal semiconductor quantum dots with tunable surface composition. *Nano Lett.* **2012**, *12*, 4465−4471.

(9) Vela, J.; Htoon, H.; Chen, Y.; Park, Y.-S.; Ghosh, Y.; Goodwin, P. M.; Werner, J. H.; Wells, N. P.; Casson, J. L.; Hollingsworth, J. A. Effect of shell thickness and composition on blinking suppression and the blinking mechanism in 'giant' CdSe/CdS nanocrystal quantum dots. *J. Biophotonics* **2010**, *3*, 706−717.

(10) Galland, C.; Ghosh, Y.; Steinbrück, A.; Sykora, M.; Hollingsworth, J. A.; Klimov, V. I.; Htoon, H. Two Types of Luminescence Blinking Revealed by Spectroelectrochemistry of Single Quantum Dots. *Nature* **2011**, *479*, 203−207.

(11) Zhang, A.; Dong, C.; Liu, H.; Ren, J. Blinking behavior of CdSe/CdS quantum dots controlled by alkylthiols as surface trap modifiers. *J. Phys. Chem. C* **2013**, *117*, 24592−24600.

(12) Chen, O.; Zhao, J.; Chauhan, V. P.; Cui, J.; Wong, C.; Harris, D. K.; Wei, H.; Han, H.-S.; Fukumura, D.; Jain, R. K.; Bawendi, M. G. Compact high-quality CdSe−CdS core−shell nanocrystals with narrow emission linewidths and suppressed blinking. *Nat. Mater.* **2013**, *12*, 445−451.

(13) Shen, H.; Lin, Q.; Cao, W.; Yang, C.; Shewmon, N. T.; Wang, H.; Niu, J.; Li, L. S.; Xue, J. Efficient and long-lifetime full-color light-emitting diodes using high luminescence quantum yield thick-shell quantum dots. *Nanoscale* **2017**, *9*, 13583−13591.

(14) Smith, A. M.; Nie, S. Chemical analysis and cellular imaging with quantum dots. *Analyst* **2004**, *129*, 672−677.

(15) Klimov, V. I. *Semiconductor and Metal Nanocrystals*; CRC Press, 2004; pp 1−500.

(16) Makarov, N. S.; Lau, P. C.; Olson, C.; Velizhanin, K. A.; Solntsev, K. M.; Kieu, K.; Kilina, S.; Tretiak, S.; Norwood, R. A.; Peyghambarian, N.; Perry, J. W. Two-photon absorption in CdSe colloidal quantum dots compared to organic molecules. *ACS Nano* **2014**, *8*, 12572−12586.

(17) Yoffe, A. D. Semiconductor quantum dots and related systems: electronic, optical, luminescence and related properties of low dimensional systems. *Adv. Phys.* **2001**, *50*, 1−208.

(18) Kilina, S.; Kilin, D.; Tretiak, S. Light-driven and phonon-assisted dynamics in organic and semiconductor nanostructures. *Chem. Rev.* **2015**, *115*, 5929−5978.

(19) Kilina, S. V.; Tamukong, P. K.; Kilin, D. S. Surface chemistry of semiconducting quantum dots: theoretical perspectives. *Acc. Chem. Res.* **2016**, *49*, 2127−2135.

(20) Orfield, N. J.; Majumder, S.; McBride, J. R.; Yik-Ching Koh, F.; Singh, A.; Bouquin, S. J.; Casson, J. L.; Johnson, A. D.; Sun, L.; Li, X.; et al. Photophysics of thermally-assisted photobleaching in "giant" quantum dots revealed in single nanocrystals. *ACS Nano* **2018**, *12*, 4206−4217.

(21) Ghosh, Y.; Mangum, B. D.; Casson, J. L.; Williams, D. J.; Htoon, H.; Hollingsworth, J. A. New insights into the complexities of shell growth and the strong influence of particle volume in nonblinking "giant" core/shell nanocrystal quantum dots. *J. Am. Chem. Soc.* **2012**, *134*, 9634−9643.

(22) Mahler, B.; Spinicelli, P.; Buil, S.; Quelin, X.; Hermier, J.-P.; Dubertret, B. Towards non-blinking colloidal quantum dots. *Nat. Mater.* **2008**, *7*, 659−664.

(23) Yang, Y.; Zheng, Y.; Cao, W.; Titov, A.; Hyvonen, J.; Manders, J. R.; Xue, J.; Holloway, P. H.; Qian, L. High-efficiency light-emitting devices based on quantum dots with tailored nanostructures. *Nat. Photonics* **2015**, *9*, 259.

(24) Baker, D. R.; Kamat, P. V. Tuning the emission of CdSe quantum dots by controlled trap enhancement. *Langmuir* **2010**, *26*, 11272−11276.

(25) Dibbell, R. S.; Watson, D. F. Distance-dependent electron transfer in tethered assemblies of CdS quantum dots and TiO2 nanoparticles. *J. Phys. Chem. C* **2009**, *113*, 3139−3149.

(26) Kasuya, A.; Sivamohan, R.; Barnakov, Y. A.; Dmitruk, I. M.; Nirasawa, T.; Romanyuk, V. R.; Kumar, V.; Mamykin, S. V.; Tohji, K.; Jeyadevan, B.; Shinoda, K.; Kudo, T.; Terasaki, O.; Liu, Z.; Belosludov, R. V.; Sundararajan, V.; Kawazoe, Y. Ultra-stable nanoparticles of CdSe revealed from mass spectrometry. *Nat. Mater.* **2004**, *3*, 99−102.

(27) Beri, R. K.; Khanna, P. K.; Singh, V.; Mehta, B. R. "Yellow Emitting" Magic-Size Cadmium Selenide Nanocrystals Via a Simplified Spray Pyrolysis Method. *Curr. Appl. Phys.* **2011**, *11*, 809−811.

(28) Cui, P.; Jabed, M.; Vogel, D. J.; Kilina, S. Phonon-Mediated Ultrafast Hole Transfer from Photoexcited CdSe Quantum Dots to Black Dye. *Computational Photocatalysis: Modeling of Photophysics and Photochemistry at Interfaces*; ACS Publications, 2019; pp 137−156.
(29) Dmitruk, I.; Belosludov, R. V.; Dmytruk, A.; Noda, Y.; Barnakov, Y.; Park, Y.-S.; Kasuya, A. Experimental and Computational Studies of the Structure of CdSe Magic-Size Clusters. *J. Phys. Chem. A* **2020**, *124*, 3398−3406.
(30) Munro, A. M.; Chandler, C.; Garling, M.; Chai, D.; Popovich, V.; Lystrom, L.; Kilina, S. Phenyldithiocarbamate Ligands Decompose During Nanocrystal Ligand Exchange. *J. Phys. Chem. C* **2016**, *120*, 29455−29462.
(31) Tamukong, P. K.; Peiris, W. D. N.; Kilina, S. Computational insights into CdSe quantum dots' interactions with acetate ligands. *Phys. Chem. Chem. Phys.* **2016**, *18*, 20499−20510.
(32) Cui, P.; Tamukong, P. K.; Kilina, S. Effect of Binding Geometry on Charge Transfer in CdSe Nanocrystals Functionalized by N719 Dyes to Tune Energy Conversion Efficiency. *ACS Appl. Nano Mater.* **2018**, *1*, 3174−3185.
(33) Kilina, S. V.; Kilin, D. S.; Prezhdo, O. V. Breaking the phonon bottleneck in PbSe and CdSe quantum dots: time-domain density functional theory of charge carrier relaxation. *ACS Nano* **2009**, *3*, 93−99.
(34) Nguyen, K. A.; Day, P. N.; Pachter, R. Understanding structural and optical properties of nanoscale CdSe magic-size quantum dots: insight from computational prediction. *J. Phys. Chem. C* **2010**, *114*, 16197−16209.
(35) Kilina, S.; Ivanov, S.; Tretiak, S. Effect of surface ligands on optical and electronic spectra of semiconductor nanoclusters. *J. Am. Chem. Soc.* **2009**, *131*, 7717−7726.
(36) Fischer, S. A.; Crotty, A. M.; Kilina, S. V.; Ivanov, S. A.; Tretiak, S. Passivating ligand and solvent contributions to the electronic properties of semiconductor nanocrystals. *Nanoscale* **2012**, *4*, 904−914.
(37) Mahan, G. D. Local-field corrections to coulomb interactions. *Phys. Rev.* **1967**, *153*, 983.
(38) Puzder, A.; Williamson, A. J.; Zaitseva, N.; Galli, G.; Manna, L.; Alivisatos, A. P. The Effect of Organic Ligand Binding on the Growth of CdSe Nanoparticles Probed by Ab Initio Calculations. *Nano Lett.* **2004**, *4*, 2361−2365.
(39) Hedrick, M. M.; Mayo, M. L.; Badaeva, E.; Kilina, S. First-Principles Studies of the Ground- and Excited-State Properties of Quantum Dots Functionalized by Ru(II)−Polybipyridine. *J. Phys. Chem. C* **2013**, *117*, 18216−18224.
(40) Kilina, S.; Cui, P.; Fischer, S. A.; Tretiak, S. Conditions for Directional Charge Transfer in CdSe Quantum Dots Functionalized by Ru(II) Polypyridine Complexes. *J. Phys. Chem. Lett.* **2014**, *5*, 3565−3576.
(41) Li, W.; Lu, T.-F.; Ren, W.; Deng, L.; Zhang, X.; Wang, L.; Tang, J.; Kuznetsov, A. E. Influence of an exciton-delocalizing ligand on the structural, electronic, and spectral features of the Cd33S33 quantum dot: insights from computational studies. *J. Mater. Chem. C* **2018**, *6*, 8751−8761.
(42) Frisch, M. J.; Trucks, G. W.; Schlegel, H. B.; Scuseria, G. E.; Robb, M. A.; Cheeseman, J. R.; Scalmani, G.; Barone, V.; Petersson, G. A.; Nakatsuji, H.; et al. *Gaussian 16*, Revision C.01; Gaussian, Inc.: Wallingford CT, 2016.
(43) Perdew, J. P.; Burke, K.; Ernzerhof, M. Generalized gradient approximation made simple. *Phys. Rev. Lett.* **1996**, *77*, 3865.
(44) Hay, P. J.; Wadt, W. R. Ab initio effective core potentials for molecular calculations. Potentials for the transition metal atoms Sc to Hg. *J. Chem. Phys.* **1985**, *82*, 270−283.
(45) Wadt, W. R.; Hay, P. J. Ab initio effective core potentials for molecular calculations. Potentials for main group elements Na to Bi. *J. Chem. Phys.* **1985**, *82*, 284−298.
(46) Krishnan, R.; Binkley, J. S.; Seeger, R.; Pople, J. A. Self-consistent molecular orbital methods. XX. A basis set for correlated wave functions. *J. Chem. Phys.* **1980**, *72*, 650−654.
(47) Hariharan, P. C.; Pople, J. A. The influence of polarization functions on molecular orbital hydrogenation energies. *Theor. Chim. Acta* **1973**, *28*, 213−222.
(48) Clark, T.; Chandrasekhar, J.; Spitznagel, G. n. W.; Schleyer, P. V. R. Efficient diffuse function-augmented basis sets for anion calculations. III. The 3-21+G basis set for first-row elements, Li−F. *J. Comput. Chem.* **1983**, *4*, 294−301.
(49) Francl, M. M.; Pietro, W. J.; Hehre, W. J.; Binkley, J. S.; Gordon, M. S.; DeFrees, D. J.; Pople, J. A. Self-consistent molecular orbital methods. XXIII. A polarization-type basis set for second-row elements. *J. Chem. Phys.* **1982**, *77*, 3654−3665.
(50) Gill, P. M. W.; Johnson, B. G.; Pople, J. A.; Frisch, M. J. The performance of the Becke−Lee−Yang−Parr (B-LYP) density functional theory with various basis sets. *Chem. Phys. Lett.* **1992**, *197*, 499−505.
(51) Cossi, M.; Barone, V.; Cammi, R.; Tomasi, J. Ab initio study of solvated molecules: a new implementation of the polarizable continuum model. *Chem. Phys. Lett.* **1996**, *255*, 327−335.
(52) Barone, V.; Cossi, M.; Tomasi, J. Geometry optimization of molecular structures in solution by the polarizable continuum model. *J. Comput. Chem.* **1998**, *19*, 404−417.
(53) Albert, V. V.; Ivanov, S. A.; Tretiak, S.; Kilina, S. V. Electronic structure of ligated CdSe clusters: dependence on DFT methodology. *J. Phys. Chem. C* **2011**, *115*, 15793−15800.
(54) Kasha, M. Characterization of electronic transitions in complex molecules. *Discuss. Faraday Soc.* **1950**, *9*, 14−19.
(55) Gong, K.; Kelley, D. F.; Kelley, A. M. Resonance Raman excitation profiles of CdS in pure CdS and CdSe/CdS core/shell quantum dots: CdS-localized excitons. *J. Chem. Phys.* **2017**, *147*, 224702.
(56) Martin, R. L. Natural transition orbitals. *J. Chem. Phys.* **2003**, *118*, 4775−4777.
(57) Humphrey, W.; Dalke, A.; Schulten, K. VMD: visual molecular dynamics. *J. Mol. Graphics* **1996**, *14*, 33−38.

https://dx.doi.org/10.1021/acs.chemmater.0c03610
Chem. Mater. 2021, 33, 892−901